Higgs pair production in the four b quarks final state

Ana Luísa Moreira de Carvalho

Instituto Superior Técnico, Lisboa, Portugal

October 2018

Abstract

This article presents a feasibility study targeting the search for Higgs pairs in the $hh \to b\bar{b}b\bar{b}$ channel at a center of mass energy of $\sqrt{s} = 100$ TeV at a future hadronic circular collider, considering a high integrate luminosity. For Standard Model production of Higgs pairs, the achieved significance with a simple cut-based boosted analysis is $S/\sqrt{B} = 8.8 \pm 1.6$ (stat.) $^{+4.4}_{-3.4}$ (sys.). The change in the significance as a function of the granularity of the hadronic calorimeter is studied, targeting the optimization of the design of future detectors.

Keywords: Keyword1, Keyword2, Keyword3, Keyword4, Keyword5

1. Introduction and motivation

A lot of work is currently being put into designing and understanding the physics reach of future particle colliders. The hadronic Future Circular Collider (FCC-hh) study, led by CERN, is one of the possibilities currently being analyzed. Its baseline design consists of a 100 km ring located in the Geneva area, capable of delivering proton-proton collisions at a center of mass energy of 100 TeV. The next milestone for this project is the delivery of a Conceptual Design Report (CDR) by the end of 2018. This document should include a first cost estimate as well as a compilation of feasibility analyses that illustrate the physics potential of such an accelerator.

A particularly interesting benchmark process to be studied in future colliders is the production of pairs of Higgs bosons (or di-Higgs production). This process is sensitive to the value of the Higgs boson triple coupling, that determines the shape of the Higgs potential and therefore plays a crucial role in the electroweak symmetry breaking mechanism. The leading order Feynamn diagrams that contribute to Higgs pair production through gluon-gluon fusion are shown in figure 1. The top diagram is the one that provides sensitivity to the triple coupling.

However, searches for di-Higgs production are extremely challenging mainly because the cross section of this process is very small, of the order of tens of femtobarns (fb). Even with the entire dataset that is expected to be accumulated during the LHC lifetime, including its high luminosity upgrade, ($O(3)$ ab^{-1}), it is very unlikely that we will be able to declare the observation of this process and certainly study it in detail. Therefore, the discovery of di-Higgs production relies on future colliders, making it a key benchmark process.

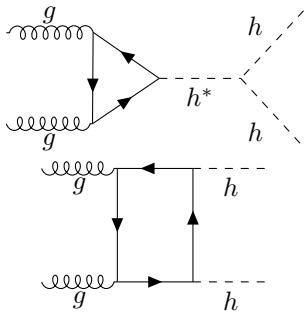

Figure 1: Feynman diagrams for the $gg \to hh$ process at leading order.

In this work we focus on the final state with four b quarks. The $h \to b\bar{b}$ decay has the largest of all Higgs branching ratios (BR), approximately 58%. Therefore this final state maximizes the cross section times branching of the $hh \to b\bar{b}b\bar{b}$ process. However, for this final state, the dominant background is multijet production through quantum chromodynamics (QCD) processes whose cross section is a lot larger than that of the signal. Nonetheless, it is a well known characteristic of QCD interactions that the partons (and jets) produced tend to have a low transverse momentum (p_T). This indicates that exploring a high p_T region of phase space could be the key to suppress the QCD multijet background. Such region is called boosted due to the high Lorentz boost of the objects involved. In this kinematic regime, traditional jet reconstruction algorithms, that establish a one to one correspondence between partons and jets, begin to fail

because the $\Delta R = \sqrt{(\Delta\phi)^2 + (\Delta\eta)^2}$ distance between the b quarks, $\Delta R(b\bar{b})$, gets increasingly small as the p_T of the mother Higgs boson, $p_T(h_1)$, increases. This is shown in figure 2. State of the art jet reconstruction techniques [1] use a single jet with a large R parameter to reconstruct both b quarks as a single jet, that is used as a *proxy* for the Higgs boson. In order to extract as much information as possible from these jets it is important to analyze its intrinsic structure, referred to as substructure. Such techniques are fairly recent and usually explore the existence of localized energy maxima inside a large-R jet (subjets). For example, a jet that contains the two b quarks coming from the decay of a Higgs boson is expected to be more compatible with the existence of two subjets than a jet produced by a QCD process.

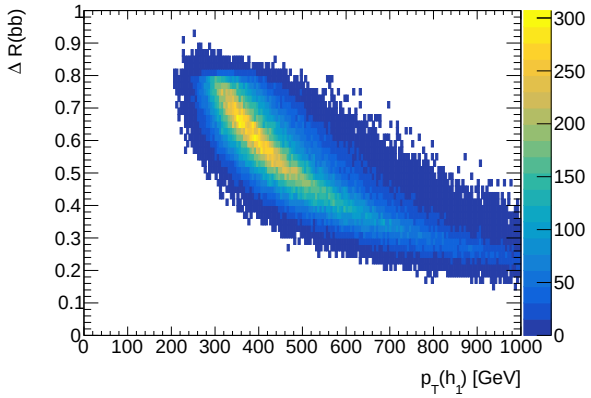

Figure 2: ΔR between the b quarks from the decay of the leading Higgs candidate as a function of its p_T.

From the point of view of detector design for the FCC-hh, as well as for future upgrades of existent detectors such as ATLAS, the granularity of the hadronic calorimeter (HCAL) is a key parameter because it greatly influences the ability of the detector to resolve the substructure of large R jets.

The main goal of this project is to use boosted di-Higgs production in the four b quarks final state as a benchmark to study the influence of the HCAL on the significance ($S/\sqrt{B}$) that can be achieved.

2. Collider experiments

2.1. The LHC and the ATLAS detector

The Large Hadron Collider (LHC) is housed by the European Organization for Nuclear Reasearch (CERN) and located beneath the Franco-Swiss boarder in the Geneva area. It consists of a 27 km ring dedicated (most of the time) to delivering proton-proton collisions at a center of mass (CM) energy of $\sqrt{s} = 13$ TeV. The two general purpose experiments, ATLAS and CMS, have a broad experimental physics program that includes searches for new physics as well as precision measurements of key properties of the Higgs boson, top quark and Z and $W^{\pm}$ bosons. The LHCb experiment is dedicated to the study of beauty particles and the ALICE experiment is optimized to study heavy ion collisions.

The ATLAS detector is a multipurpose particle physics apparatus with forward-b ackward symmetric cylindrical geometry. A combination of cartesian and cylindrical coordinates is used to describe it. The origin is defined to coincide with the interaction point. The Cartesian system is right-handed and the z axis is defined to be the direction of the beam. The x-axis points from the interaction point to the center of the LHC ring and the y-axis points upwards. The azimuthal angle, ϕ, is measured around the beam axis and the polar angle, θ, from the beam line. The pseudorapidity is defined as $\eta = \ln\tan(\theta/2)$. The inner tracking detector (ID) consists of a silicon pixel detector, a silicon microstrip detector, and a straw-tube transition radiation tracker. It is contained in a superconducting solenoid magnet that provides a 2 T magnetic field and surrounded by a high-granularity liquid-argon sampling electromagnetic calorimeter (ECAL). The ECAL covers the pseudorapidity range $|\eta| < 3.2$. The hadronic calorimetry in the pseudorapidity range $|\eta| < 1.7$ is provided by a scintillator-tile calorimeter (TileCal). For $|\eta| > 1.5$ liquid-argon calorimeters extend the pseudorapidity range to $|\eta| = 4.9$. The LAr calorimeter is divided in end-cap and forward. These cover the pseudorapidity ranges $1.5 < |\eta| < 3.2$ and $3.2 < |\eta| < 4.9$. In the end-cap the segmentation is $\Delta\eta \times \Delta\phi = 0.1 \times 0.1$ for $1.5 < |\eta| < 2.5$ and 0.2×0.2 for $2.5 < |\eta| < 3.2$. In the forward region the segmentation is $\Delta\eta \times \Delta\phi = 0.2 \times 0.2$. The muon spectrometer (MS) surrounds the calorimeters and it is the outermost layer of the detector. It is composed of Monitored Drift Tubes and Cathode Strip Chambers.

2.2. The FCC-hh

The FCC-hh baseline design consist of a of a proton-proton circular collider with a maximum CM energy of $\sqrt{s} = 100$ TeV, housed in a 100 km tunnel in the area of Geneva. It will deliver a peak luminosity of $\mathcal{L} = 30 \times 10^{34}$ cm^{-2}s^{-1} in its ultimate phase which will result in a $O(30)$ ab^{-1} per experiment. This machine will extend the research program of the LHC (and of the HL-LHC) after these have reached their full discovery potential, by around 2040.

The design of the FCC-hh baseline detector has been greatly based on that of the ATLAS and CMS experiments, in particular the central barrel. The layers and sub detectors are arranged in the same order and make use of very similar technologies. The ID detector covers the pseudorapidity range

$|\eta| < 6$ and it will be instrumented with pixel and strip detectors. The ECAL covers the pseudorapidity range $|\eta| < 6$. The proposed layout is a LAr sampling configuration with lead, glue and steal plates as absorbers. The granularity is expected to be two to four times better than for the ATLAS ECAL. The hadronic calorimeter covers the pseudorapidity range $|\eta| < 6$. It is divided in barrel, end-cap and forward, that cover the pseudorapidity ranges $|\eta| < 1.3$, $1.0 < |\eta| < 1.8$ and $2.3 < |\eta| < 6.0$, respectively. For the barrel and end-cap calorimeters, the expected segmentation $\Delta\eta \times \Delta\phi = 0.025 \times 0.025$ while for the forward calorimeter it is $\Delta\eta \times \Delta\phi = 0.05 \times 0.05$. Overall, this corresponds to approximately four times the ATLAS HCAL granularity. The MS covers the pseudorapidity range $|\eta| < 6$ and it consists of a layered structure of gas chambers.

3. State of the art

The searches performed so far for di-Higgs production covered different decay channels and targeted not only the SM production but also some BSM scenarios where this process is enhanced. None of them could achieve enough statistical significance to declare the observation of this process nor find any deviation from the SM predictions.

The most stringent limit comes from a combination of searches using up to 36.1 fb^{-1} of proton-proton collision data at a center of mass energy $\sqrt{s} = 13$ TeV, recorded with the ATLAS detector [2]. The combination is performed using the analysis searching for $hh \to b\bar{b}b\bar{b}$, $hh \to b\bar{b}\tau^+\tau^\cdot$ and $hh \to b\bar{b}\gamma\gamma$. The combined observed (expected) limit on the non-resonant Higgs boson pair cross-section is 0.22(0.35) pb at 95% confidence level (CL), which corresponds to 6.7(10.4) times the predicted SM cross-section. The ratio of the Higgs boson self-coupling to its SM expectation ($k_\lambda = \lambda_{hhh}/\lambda^{SM}_{hhh}$) is observed (expected) to be contrained at 95% CL to $-5.0 < k_\lambda < 12.1 (-5.8 < k_\lambda < 12.0)$.

Monte Carlo studies assessing the feasibility of searches for di-Higgs production at the High Luminosity LHC (HL-LHC) and at the FCC-hh have been performed. For the HL-LHC, a study including the $pp \to b\bar{b}b\bar{b}$, $pp \to b\bar{b}jj$, $pp \to jjjj$ and $pp \to t\bar{t}jjjj$ backgrounds reports a significance of $S/\sqrt{B} = 3.1$ (1.0) for an integrated luminosity of 3000 (300) fb^{-1}, considering a mean pileup of 80 [3]. The analysis is performed in three orthogonal signal categories (resolved, intermediate and boosted) and the reported significance is obtained from the combination of the three regions. This study makes use of an artificial neural network to further increase the signal-background separation. Similar studies performed by ATLAS and CMS found the $hh \to b\bar{b}\gamma\gamma$ channel to be the most sensitive to the Higgs trilinear coupling. ATLAS reports a significance of 1.06 for an integrated luminosity of 3000 fb^{-1}, which translates to a 95% CL limit on the ratio of the Higgs boson self-coupling to its SM expectation of $-0.8 < k_\lambda < 7.7$ [4]. This analysis is purely cut based and a mean pileup of $< \mu > \sim 200$ is considered.

For the FCC-hh, a recent study simulates the signal with an extra jet at generator level: $pp \to b\bar{b}b\bar{b}j$ [5]. The extra jet boosts the Higgs pair favoring a highly boosted virtual Higgs decaying to a pair of Higgs bosons which enhances the sensitivity to the Higgs trilinear coupling. Only the irreducible background, $pp \to b\bar{b}b\bar{b}j$, is considered. A significance of 6.61 is reported for an integrated luminosity of 30 ab^{-1}. No MVA techniques are applied nor pileup contribution considered.

Studies of the impact of the granularity of the calorimeters in the spatial resolving power of hadronic showers and on the resolution of jet mass and substructure variables greatly influenced the baseline design of the FCC-hh. For two Kaons with an energy of 100 GeV each and with a truth level separation equal to $\Delta R = 0.035$ it is shown that for a segmentatin of $\Delta\eta \times \Delta\phi = 0.022 \times 0.022$ both particles can be resolved in the HCAL [6]. A series of results presented in Refs. [7, 8, 9] analyze three calorimeter benchmark configurations: HCAL(ECAL) $0.1(0.025)\eta \times 0.1(0.025)\phi$, HCAL(ECAL) $0.05(0.012)\eta \times 0.05(0.012)\phi$ and HCAL(ECAL) $0.025(0.006)\eta \times 0.025(0.006)\phi$. The jet mass resolution for jets with $p_T > 3$ TeV in $t\bar{t}$ events improves by 44% and 47% for $\Delta\eta \times \Delta\phi = 0.05 \times 0.05$ and $\Delta\eta \times \Delta\phi = 0.025 \times 0.025$ cells with respect to $\Delta\eta \times \Delta\phi = 0.1 \times 0.1$. The resolution on the τ_{32} variable is also shown to increase as the granularity increases. In addition, "eflow" (particle/energy flow) jets are shown to have a better resolution on this variable than calorimeter jets. "Eflow" jets are reconstructed using information from the tracking system and from the calorimeter towers while calorimeter/tower jets do not take into account any information from the tracking. In Ref. [7] it is shown that the overlap between the distributions of the τ_{21} variable in jets with $p_T > 2.5$ TeV resulting from the decay of a W boson and in QCD jets decreases from 80% to 60% going from $\Delta\eta \times \Delta\phi = 0.1 \times 0.1$ to $\Delta\eta \times \Delta\phi = 0.005 \times 0.005$. For 20 TeV jets the change in the HCAL granularity does not significantly modify the overlap.

4. Analysis

The main backgrounds affecting di-Higgs searches in the $b\bar{b}b\bar{b}$ channel are multijet and $t\bar{t}$ production. All other sources of background, including processes involving Higgs bosons, are found to be negligible [10]. In addition to these, we also consider the irre-

ducible background ($pp \to b\bar{b}b\bar{b}$) as a separate background source.

We study the production of Higgs pairs in three different models: the SM, a dark matter (DM) model with a 1 TeV spin-0 mediator that can decay to Higgs pairs [11] and the CP-conserving Two Higgs Doublet Model (2HDM) of type II where the heavier CP-even Higgs can decay to pairs of SM-like Higgs bosons [12].

We choose the mass of the new heavy resonances to be high ($\sim$ 1 TeV) in order to increase the efficiency of the boosted selection.

4.1. Simulation setup

We simulate the signal and background Monte Carlo samples using a fast simulation workflow. MadGraph5 aMC@NLO [13] is used to compute the matrix elements of a given process. Showering and hadronization of colored particles are handled by Pythia8 [14] and the detector response is parameterized using Delphes3 [15].

The irreducible background is generated with an extra jet with $p_T > 200$ GeV at generator level $(4b+j)$. This guarantees that the pairs of b quarks are boosted enough to increase the probability of being reconstructed as a single, high p_T jet. The multijet background is simulated as $jj + 0/1/2\ j$ where j stands for a light- or b-initiated jet. To make the simulation more efficient, this background is generated in several H_T regions between $500 < H_T < 100000$, where H_T is the scalar sum of the p_T of all the partons at generator level. The $t\bar{t}$ background is simulated as $t\bar{t}+0/1/2\ j$. The sample is inclusive in the top quark and $W^{\pm}$ boson decay modes.

The BSM signal samples are simulated using MadGraph models publicly available in the FeynRules database. For the DM mediator model [11], the spin-0 mediator mass is set to 1 TeV.The cross section for the signal generated with this model is smaller than the cross section of the SM signal (approximately 0.2 pb *versus* 0.7 pb) and therefore this model is not excluded by experimental data.

For the 2HDM [12, 16], the input parameters for the scalar sector are:

$$\begin{aligned} &m_{h_1} = 125 \text{ GeV}, \quad m_{h_2} = 900 \text{ GeV}, \\ &m_{h_3} = 850 \text{ GeV}, \quad m_{hc} = 800 \text{ GeV} \\ &mix_{h_2} = mix_{h_3} = 0 \\ &mix_{h_1} = \frac{\pi}{2} - (\beta - \alpha) \simeq 0.035 \\ &l_2 \simeq 0.27, \quad l_3 \simeq 9.46, \quad l_7 \simeq 0.46, \end{aligned} \tag{1}$$

where $m_{h_1}, m_{h_2}, m_{h_3}$ and m_{h_c} are the masses of the three neutral scalars and of the charged scalar, respectively. The mixing angles between the neutral scalars are given by mix_{h_2}, mix_{h_3} and mix_h, where we have chosen $\beta = \frac{\pi}{4}$ and $\alpha = -0.75$. $l_{2,3,7}$ are the quartic coupling of the Higgs potential. All parameters are given in the Higgs basis. Regarding the Yukawa sector, we consider the type II model. The real part of the Yukawa matrices of the coupling of h_2 to down (GDR) and up-type (GUR) quarks are given by [12]:

$$\begin{aligned} GDR &= \text{diag}\left(0, 0, \frac{m_b\sqrt{2}\tan(\beta)}{v}\right), \\ GUR &= \text{diag}\left(0, 0, \frac{m_b\sqrt{2}}{v\tan(\beta)}\right), \end{aligned} \tag{2}$$

where $m_b = 4.7$ GeV and $m_t = 172$ GeV are the masses of the bottom and top quarks. All other matrices are null.

Different detector configurations were implemented in Delphes3. The granularity of the HCAL was the main study parameter. Starting from the FCC-hh baseline detector, five HCAL granularity benchmark configurations were tested:

1. ATLAS HCAL granularity;
2. Starting from the ATLAS HCAL configuration we increase the granularity in $|\eta|$ by a factor of four, in the pseudorapidity range $\eta < 1.7$ which corresponds to the TileCal region;
3. Starting from the FCC HCAL configuration we decrease the granularity in ϕ by a factor of two, in the entire pseudorapidity range covered by the HCAL;
4. FCC HCAL default granularity;
5. Starting from the FCC HCAL configuration we increase the granularity in η and in ϕ by a factor of two, in the entire pseudorapidity range covered by the HCAL.

These configurations are summarized in table 1. In addition, we also passed the same generator level samples through the default ATLAS detector simulation in Delphes. The HCAL granularity is the one that is indicate in the second line of table 1 but the other detectors parameters, such as the radius, magnetic field, tracking resolutions are the ones that are implemented in the default ATLAS Delphes card.

4.2. Event selection

The event selection targets the boosted kinematic regime in which both Higgs bosons are reconstructed using large-R jets. The expected event topology is illustrated in figure 3.

The events are reconstructed using particle flow (or calorimeter) jets with $R = 0.8$ clustered with the anti-k_T algorithm. The events are required to have

Config.	$\Delta\eta \times \Delta\phi$	η range
1	0.1×0.1	$\lvert\eta\rvert < 2.5$
	0.2×0.2	$2.5 < \lvert\eta\rvert < 5.0$
2	0.025×0.1	$\lvert\eta\rvert < 1.7$
	0.1×0.1	$1.7 < \lvert\eta\rvert < 2.5$
	0.2×0.2	$2.5 < \lvert\eta\rvert < 5.0$
3	0.025×0.05	$\lvert\eta\rvert < 2.5$
	0.05×0.1	$2.5 < \lvert\eta\rvert < 6.0$
4	0.025×0.025	$\lvert\eta\rvert < 2.5$
	0.05×0.05	$2.5 < \lvert\eta\rvert < 6.0$
5	0.0125×0.0125	$\lvert\eta\rvert < 2.5$
	0.025×0.025	$2.5 < \lvert\eta\rvert < 6.0$

Table 1: Summary of the benchmark granularity configurations of the HCAL.

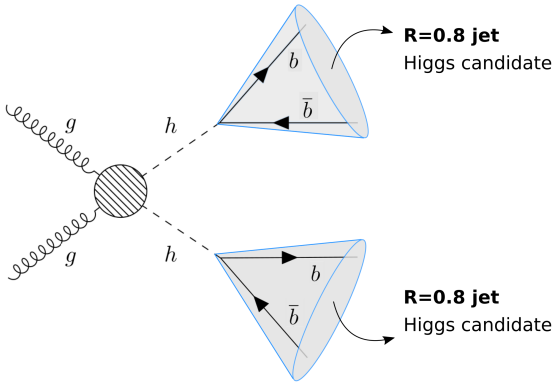

Figure 3: Event topology targeted by the boosted analysis region.

at least two jets. Each jet is required to have two subjets, both b-tagged. In addition, both jets are required to have $p_T > 200$ GeV. These cuts consist of the event pre-selection.

The b-tagging is implemented using truth level information. The b-tagging and mis-tagging efficiencies are extracted from the FCC-hh detector default Delphes card, implemented by the FCC-hh study group. They depend on the p_T and η of the jets. The b-tagging efficiency and the c- and light-jet mis-tag rates are of the order of 85%, 5% and 1%, respectively.

The event selection is described in the following paragraphs. The value of the cuts follow from a simple optimization, done by scanning over a range of possible cut values. This scan is done individually for each of the variables considered. We choose the cut value that maximizes the significance, $S/\sqrt{B}$.

We require

$$p_T(h_1) > 300 \text{ GeV}, \quad p_T(hh) > 100 \text{ GeV} \tag{3}$$

where $p_T(h_1)$, $p_T(hh)$ are the transverse momenta of the leading Higgs candidate and of the pair of Higgs candidates, whose distributions can be found in figures 4(a) and 4(b), respectively. These cuts help suppress multijet background whose p_T distributions fall more steeply than that of the signal. A requirement on the maximum value of the N-subjetiness variable [17] of the leading and subleading Higgs candidates, $\tau_{21}(h_1, h_2)$, is imposed to further reject jets that are not consistent with a two-prong substructure:

$$\tau_{21}(h_1, h_2) < 0.4. \tag{4}$$

These cuts work as a set of Higgs-tagging criteria, suppressing fake Higgs jets. The distribution of this variable for the leading Higgs is shown in figure 5(a). For the signal, the distribution is shifted to lower values. Since high-mass resonances tend to produce more central jets than multijet background processes, we require:

$$|\eta(hh)| < 1.5, \tag{5}$$

where $\Delta\eta(hh)$ is the difference between the pseudo-rapidities of the two Higgs candidates. This distribution is shown in figure 5(b). We place an additional requirement on the second Fox Wolfram momentum [18] of the leading Higgs candidate, $H_2(h_1)$, to further suppress $t\bar{t}$ contamination

$$H_2(h_1) < 0.2. \tag{6}$$

This distribution is shown in figure 6(a) where the large $t\bar{t}$ contribution is visible at values close to zero. Events are selected if the softdrop masses, M_{SD}, of the large-R jets are consistent with the SM Higgs boson mass

$$(100 < M_{SD}(h_1, h_2) < 135) \text{ GeV} \tag{7}$$

This distribution is shown in figure 6(b), for the leading Higgs candidate.

4.3. Systematic uncertainties

The sources of systematic uncertainty considered are those affecting the signal b-tagging efficiency and the normalization of the backgrounds. These are the dominant uncertainties in the search for boosted $hh \to b\bar{b}b\bar{b}$ [10] and rough estimates of their size are extracted from the literature. In the four b-tags signal region, the uncertainty on the b-tagging is of the order of 30% [10]. For the normalization of the QCD multijet and $t\bar{t}$ backgrounds we consider uncertainties of 50% and 20%, respectively [19].

The b-tagging uncertainty is implemented by varying the number of signal events up and down by 30%. The normalization of the QCD multijet ($4b + j$ and $jj + 0/1/2\ j$) and $t\bar{t}$ is varied independently by the corresponding factors. The systematic uncertainties are considered to be uncorrelated and therefore the variations to the nominal value of $S/\sqrt{B}$ are added in quadrature.

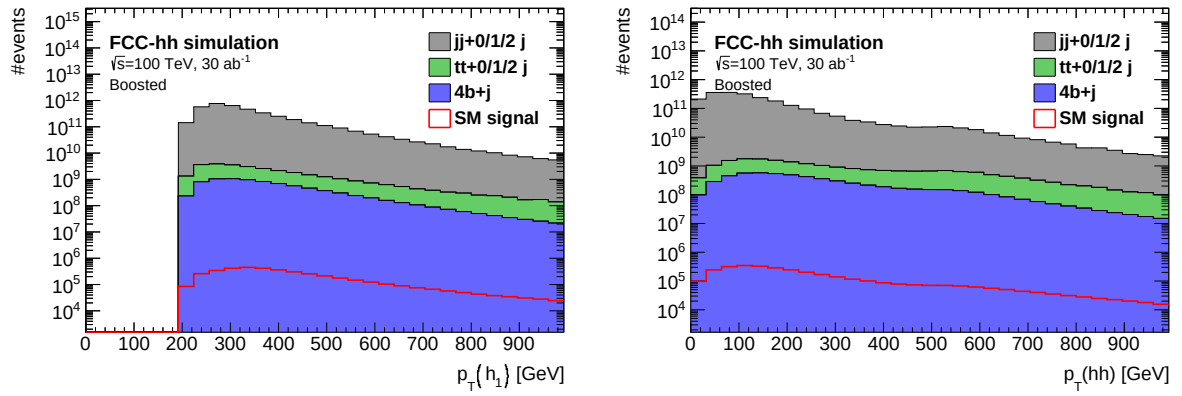

(a) (b)

Figure 4: (a) p_T distributions of the leading Higgs candidate, $p_T(h_1)$, after the pre-selection cuts, (b) p_T distribution of the Higgs pair, $p_T(hh)$, after the cut on $p_T(h_1) > 300$ GeV.

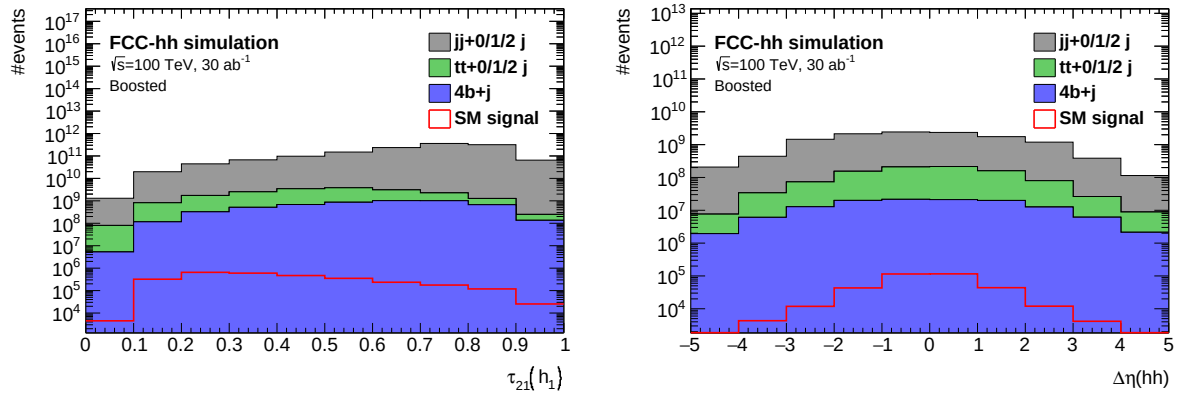

(a) (b)

Figure 5: (a) τ_{21} distribution for the leading Higgs candidate, $\tau_{21}(h_1)$, after the cut on $p_T(hh) > 100$ GeV, (b) Distribution of the $\Delta\eta$ between the two Higgs candidates, $\Delta\eta(hh)$, after the cuts on $\tau_{21}(h_1, h_2) < 0.4$.

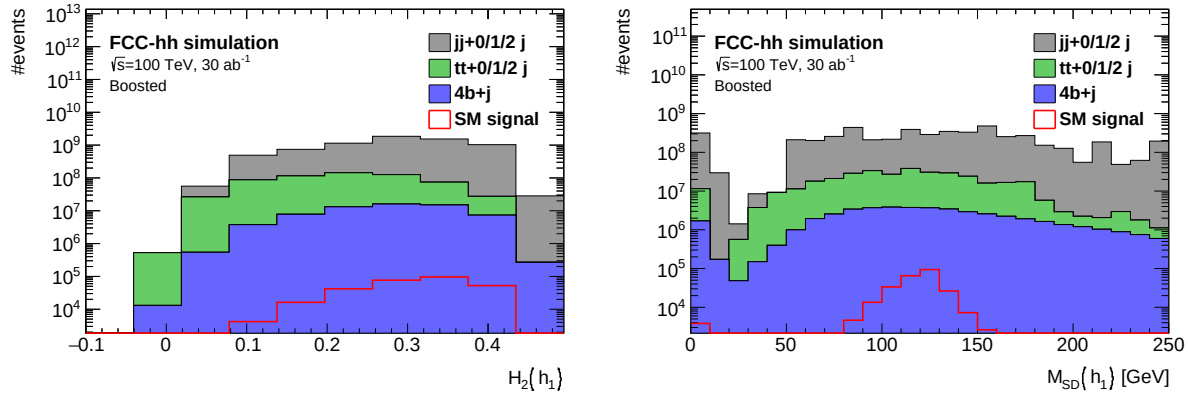

(a) (b)

Figure 6: (a) Distribution of the second Fox-Wolfram momentum of the leading Higgs candidate, $H_2(h_1)$, after the cut $|\Delta\eta(hh)| < 1.5$, (b) Softdrop mass distribution for the leading Higgs candidate, $M_{SD}(h_1)$, after the cut $H_2(h_1) > 0.2$.

5. Results

The analysis described in section 4 was developed and optimized using samples simulated with the default FCC-hh detector implementation. The results are reported in terms of the significance, $S/\sqrt{B}$, that was achieved (section 5.1). The same analysis is applied to the different detector configurations (described in section 4.1) and the results compared in terms of significance and signal efficiency (section 5.2).

5.1. Higgs pair discovery potential at the FCC-hh

Considering the SM signal production the achieved significance is

$$(S/\sqrt{B})_{SM} = 8.8 \pm 1.6 \text{ (stat.) } ^{+4.4}_{-3.4} \text{ (sys.)} \quad (8)$$

for an integrated luminosity of 30 ab^{-1}. The value of the significance is above the observation threshold which indicates that the full dataset expected to be accumulated in the FCC-hh should be enough to declare the observation (or to exclude) the production of Higgs pairs as predicted by the SM.

For the 1 TeV DM mediator signal, the significance is 2.3 ± 0.4 (stat.) $^{+1.2}_{-0.9}$ (sys.) for $\mathcal{L} = 30$ ab^{-1} which makes it a challenging and probably inaccessible benchmark. For the 2HDM signal the achieved significance is

$$(S/\sqrt{B})_{2HDM} = 16.9 \pm 3.0 \text{ (stat.) } ^{+8.5}_{-6.6} \text{ (sys.)} \quad (9)$$

for $\mathcal{L} = 30$ ab^{-1}, making it a very interesting benchmark model from the point of view of enhancing Higgs pair production with respect to the SM.

The signal efficiency is higher for both BSM models than for the SM, because the masses of the new heavy resonances were chosen to be large (O(1 TeV)), so as to produce highly boosted Higgs pairs. For the SM the efficiency is approximately 0.4%. It increases to 0.5% for the DM mediator model and to 1.7% for the 2HDM.

5.2. Granularity studies for future colliders

Figure 7 shows the signal efficiency (in percentage) as a function of the detector configuration. The left most point corresponds to the ATLAS detector and the right most point to the FCC-hh detector with a granularity twice as good in η and ϕ (configuration 5 in table 1). The points in between are ordered by increasing granularity of the HCAL. All other plots that show some quantity as a function of detector configuration follow the same convention. For all signal models, the efficiency increases as the granularity of the HCAL increases. It increases by approximately 30% from the first to the last points.

Figures 8 and 9 show the significance as a function of the detector configuration for the SM signal model and for the 2HDM, respectively. Triangular markers represent analyses that were performed using pure HCAL jets, while square markers represent analysis performed using energy flow jets.

For energy flow jets the change in significance is very mild. It varies by approximately 30% between the first and last points, for both signal models. It becomes more pronounced when using pure calorimeter jets. In this case, it varies by approximately 70% (55%) between the first and last points for the SM (2HDM) signal. However, when using calorimeter jets, the achieved significance is always smaller (for the same detector configuration) because we are not using information from the tracking system. This is verified for both the SM and 2HDM signals. These results indicate that when using energy flow jets the tracking system is dominating the jet reconstruction.

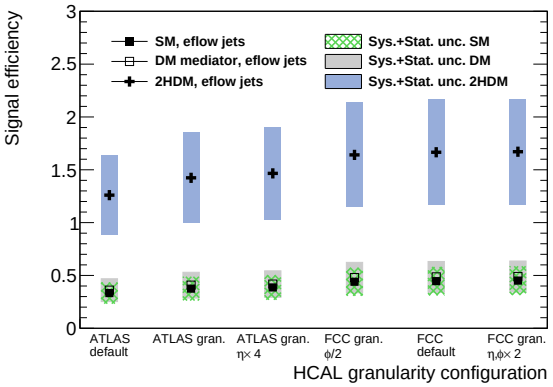

Figure 7: Signal efficiency in percentage as a function of the detector configuration. The statistical error bars are drawn but are smaller than the markers.

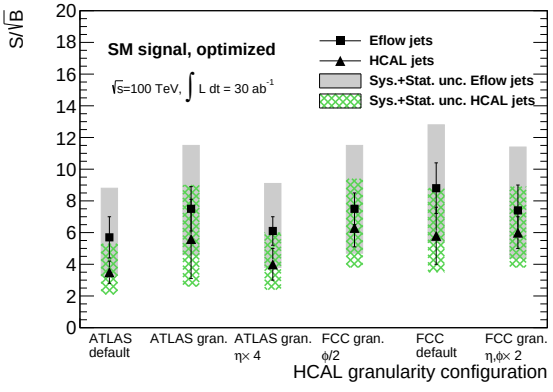

Figure 8: $S/\sqrt{B}$ as a function of the detector configuration for the SM signal model. The square (triangular) markers refer to values obtained using particle flow (calorimeter) jets.

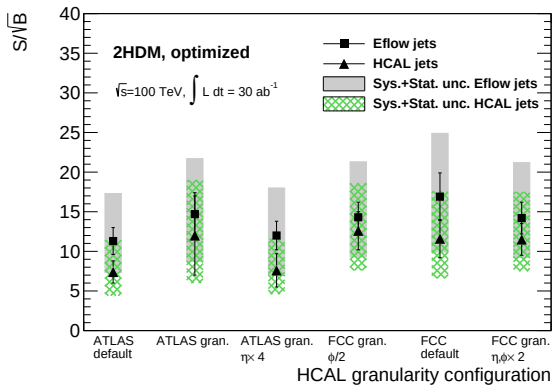

Figure 9: $S/\sqrt{B}$ as a function of the detector configuration for the 2HDM signal model. The square (triangular) markers refer to values obtained using particle flow (calorimeter) jets.

6. Conclusions

This article presents a feasibility study targeting the search for Higgs pair production in the $pp \to hh \to b\bar{b}b\bar{b}$ channel at a center of mass energy of $\sqrt{s} = 100$ TeV. The analysis is based on rectangular cuts on kinematic and substructure variables, and targets a boosted event topology. The main backgrounds are QCD multijet and $t\bar{t}$ production. The impact of the granularity of the hadronic calorimeter on the achieved significance was studied.

Three signal models are investigated: SM, 1 TeV DM spin-0 mediator and CP-conserving type II 2HDM with $m_H = 900$ GeV. Due to the small cross section, the DM mediator model originates a significance of the order of 2, making it a very challenging and probably unaccessible background.

For the FCC-hh, the significances achieved for the SM and 2HDM signal modes were $(S/\sqrt{B})_{SM} = 8.8 \pm 1.6$ (stat.) $^{+4.4}_{-3.4}$ (sys.) and $(S/\sqrt{B})_{2HDM} = 16.9 \pm 3.0$ (stat.) $^{+8.5}_{-6.6}$ (sys.), respectively, for an integrated luminosity of $\mathcal{L} = 30$ ab^{-1}. These values are above the 5σ threshold which indicates that the total dataset that is expected to be collected at the FCC-hh should be enough to observe (or exclude) the production of Higgs pairs in these models.

For particle-flow jets, the efficiency of the signal increases as the granularity of the HCAL increases. It varies by approximately 30% between the ATLAS detector configuration and the detector configuration with twice the granularity of the FCC baseline detector in η and ϕ. It is harder to discern such a clear tendency for the significance because the statistical fluctuations are large, which is due to the large statistical weight of the multijet background. Nonetheless, for particle flow (calorimeter) jets, the significance varies by approximately 30% (70%), for the SM signal model.

As future work, performing similar studies using different benchmark processes and full detector simulation seems to be of the utmost importance in order to optimize the design of future detectors.

Acknowledgements

The author would like to thank Ricardo Gonçalo for supervising this work, contributing with invaluable scientific advise and ultimately making it possible. The author would also like to acknowledge the support of the Fundação para a Ciência e Tecnologia through the CERN/FIS-PAR/0008/2017 grant.

References

[1] G. A. et al, Performance of jet substructure techniques for large-r jets in proton-proton collisions at $\sqrt{s} = 7$ tev using the atlas detector, Journal of High Energy Physics 2013 (9). doi:10.1007/JHEP09(2013)076.
URL https://doi.org/10.1007/JHEP09(2013)076

[2] M. Aaboud, et al., Combination of searches for heavy resonances decaying into bosonic and leptonic final states using 36 fb^{-1} of proton-proton collision data at $\sqrt{s} = 13$ TeV with the ATLAS detectorarXiv:1808.02380.

[3] J. K. Behr, D. Bortoletto, J. A. Frost, N. P. Hartland, C. Issever, J. Rojo, Boosting Higgs pair production in the $b\bar{b}b\bar{b}$ final state with multivariate techniques, Eur. Phys. J. C76 (7) (2016) 386. arXiv:1512.08928, doi:10.1140/epjc/s10052-016-4215-5.

[4] Study of the double Higgs production channel $H(\to b\bar{b})H(\to \gamma\gamma)$ with the ATLAS experiment at the HL-LHC, Tech. Rep. ATL-PHYS-PUB-2017-001, CERN, Geneva (Jan 2017).
URL https://cds.cern.ch/record/2243387

[5] S. Banerjee, C. Englert, M. L. Mangano, M. Selvaggi, M. Spannowsky, hh + jet production at 100 TeV, Eur. Phys. J. C78 (4) (2018) 322. arXiv:1802.01607, doi:10.1140/epjc/s10052-018-5788-y.

[6] S. V. Chekanov, M. Beydler, A. V. Kotwal, L. Gray, S. Sen, N. V. Tran, S. S. Yu, J. Zuzelski, Initial performance studies of a general-purpose detector for multi-TeV physics at a 100 TeV pp collider, JINST 12 (06) (2017) P06009. arXiv:1612.07291, doi:10.1088/1748-0221/12/06/P06009.

[7] S. Chekanov, Boosted jets in high-granularity calorimeter at a 100 TeV pp collider, bOOST 2017 (2017).

[8] S. Chekanov, Physics requirements for a Hadron Calorimeter for a 100 TeV proton-proton collider, fCC week 2015 (2015).

[9] S. Chekanov, Simulation of a high-granular hadronic calorimeter for multi-TeV physics, fCC week 2016 (2016).

[10] M. Aaboud, et al., Search for pair production of Higgs bosons in the $b\bar{b}b\bar{b}$ final state using proton-proton collisions at $\sqrt{s} = 13$ TeV with the ATLAS detectorarXiv:1804.06174.

[11] H. C. van de Hulst, E. Raimond, H. van Woerden, Rotation and density distribution of the Andromeda nebula derived from observations of the 21-cm line 14 (1957) 1.

[12] T. general Two-Higgs-Doublet Model, C. degrande, c. duhr, m. herquet (2018). URL `http://feynrules.irmp.ucl.ac.be/wiki/2HDM`

[13] J. Alwall, M. Herquet, F. Maltoni, O. Mattelaer, T. Stelzer.

[14] T. Sjostrand, S. Mrenna, P. Z. Skands, A Brief Introduction to PYTHIA 8.1, Comput. Phys. Commun. 178 (2008) 852–867. arXiv:0710.3820, doi:10.1016/j.cpc.2008.01.036.

[15] J. de Favereau, C. Delaere, P. Demin, A. Giammanco, V. Lematre, A. Mertens, M. Selvaggi, DELPHES 3, A modular framework for fast simulation of a generic collider experiment, JHEP 02 (2014) 057. arXiv:1307.6346, doi:10.1007/JHEP02(2014)057.

[16] C. Degrande, Automatic evaluation of UV and R2 terms for beyond the Standard Model Lagrangians: a proof-of-principle, Comput. Phys. Commun. 197 (2015) 239–262. arXiv:1406.3030, doi:10.1016/j.cpc.2015.08.015.

[17] J. Thaler, K. Van Tilburg, Identifying Boosted Objects with N-subjettiness, JHEP 03 (2011) 015. arXiv:1011.2268, doi:10.1007/JHEP03(2011)015.

[18] C. Chen, New approach to identifying boosted hadronically-decaying particle using jet substructure in its center-of-mass frame, Phys. Rev. D85 (2012) 034007. arXiv:1112.2567, doi:10.1103/PhysRevD.85.034007.

[19] C. Helsens, Heavy resonances at 100TeV (2018).